THE AMERICAN SOCIETY OF MECHANICAL ENGINEERS
345 E. 47th St., New York, N.Y. 10017

94-GT-5

AN EXPERIMENTAL INVESTIGATION OF STATOR INDUCED UNSTEADINESS ON CENTRIFUGAL IMPELLER OUTFLOW

Marina Ubaldi, Pietro Zunino, Giovanna Barigozzi, and Andrea Cattanei
Dipartimento di Ingegneria Energetica
Università di Genova
Genova, Italy

ABSTRACT

Detailed flow measurements were taken in a centrifugal turbomachine model to investigate the aerodynamic influence of the vaned diffuser on the impeller flow.

The model consists of an unshrouded centrifugal impeller with backswept blades and a rotatable vaned diffuser which enables a continuous variation of the vaned diffuser location with respect to the measuring points.

Phase locked ensemble averaged velocity components have been measured with hot wire probes at the impeller outlet for 30 different relative positions of the probe with respect to the diffuser vanes. The data also include the distribution of the ensemble averaged static pressure at the impeller front end, taken by means of miniature fast response pressure transducers flush mounted at the impeller stationary casing. By circumferentially averaging the results obtained for the different circumferential probe locations, the periodically perturbed impeller flow has been split into a relative steady flow and a stator generated unsteadiness.

The results for the different probe positions have also been correlated in time to obtain instantaneous flow field images in the relative frame, which provide information on the various aspects of the diffuser vane upstream influence on the relative flow leaving the impeller.

NOMENCLATURE

b	impeller blade span
c	absolute velocity
C_p	static pressure coefficient $C_p = 2(p\text{-}p_0)/\rho U_2^2$
D_2	impeller outlet diameter
G_i	impeller circumferential pitch
l	chord length
p	static pressure
p_t	total pressure
Q	flow rate
r	radial coordinate
R_n	meridional curvature radius
t	time
T_i	impeller blade passing period
u	peripheral velocity
U_2	peripheral velocity at the impeller outlet
w	relative velocity
y_i	circumferential coordinate in the relative frame
z	axial coordinate
z_d	number of diffuser vanes
z_i	number of impeller blades
β	angle between the blade to blade relative velocity and the radial direction
β'	impeller blade angle with radial direction
γ	angle between the relative velocity and the blade to blade velocity
ν	kinematic viscosity
ρ	fluid density
θ	angular coordinate
φ	flow rate coefficient $\varphi = 4Q/(U_2\pi D_2^2)$
ψ	total pressure rise coefficient $\psi = 2(p_{t4}\text{-}p_{t0})/\rho U_2^2$
ω	angular velocity

Subscripts

d	relative to the diffuser
i	relative to the impeller
m	relative to the measuring point
r	in the radial direction
u	in the tangential direction
z	in the axial direction
0	in the suction pipe
1	at the impeller leading edge
2	at the impeller outlet
3	at the diffuser inlet
4	at the diffuser outlet

Superscripts

'	unsteady quantity
~	ensemble average
–	circumferential average

Presented at the International Gas Turbine and Aeroengine Congress and Exposition
The Hague, Netherlands — June 13–16, 1994
This paper has been accepted for publication in the Transactions of the ASME
Discussion of it will be accepted at ASME Headquarters until September 30, 1994

INTRODUCTION

Flow unsteadiness generated by rotor-stator aerodynamic interaction affects aerodynamic, thermal and structural performance of turbomachinery components. Aerodynamic interaction takes place mainly through two distinct mechanisms: wake and potential flow effects (Dring et al., 1982).

The wake viscous effect originates from the impingement and the convection of wakes shed from the preceding row through the successive blade row in relative motion. The periodic striking of turbulent wake segments determines a complex unsteady flow field which influences the onset of the boundary layer transition on the downstream blades (e. g. Pfeil et al., 1983; Hodson, 1985; La Graff et al., 1989; Liu and Rodi, 1992).

The potential flow effect is induced by the interaction of the inviscid flow fields generated by the adjacent blade rows in relative motion. It extends in both upstream and downstream directions, with a larger effect on the upstream row. However, the rate of decay of the potential perturbation is fast and the associated effect appears significant only in case of small gaps between adjacent rows.

Due to the important practical implications and the inherent complexity of the interaction phenomena, a large number of detailed experimental investigations are reported in literature. Most of these efforts concern the analysis of wake generated unsteady flows in axial turbomachines, either compressors (e. g. Zierke and Okiishi, 1982; Dunker et al., 1983; Suder et al., 1987; Hathaway et al., 1987; Poensgen and Gallus, 1990a, 1990b; Schulz et al., 1990)) or turbines (e. g. Binder et al. 1985, 1989; Zeschky and Gallus, 1991). Dring et al. (1982) and Joslyn et al. (1983) have analysed in detail both wake generated and upstream potential flow effects in a large-scale, axial flow, turbine model.

Investigations dealing with rotor-stator interaction in centrifugal turbomachines are less numerous and, in general, concern both interaction mechanisms (e. g. Krain, 1981; Inoue and Cumpsty, 1984; Arndt et al., 1990). Since the mixing process that rotor blade wakes undergo is very fast and radial gaps between rotors and vaned diffusers are small, in centrifugal machines viscous and potential flow effects become comparable.

To study basic fluid dynamic phenomena, including aerodynamic rotor-stator interaction, a simplified model of centrifugal turbomachine with rotatable vaned diffuser has been designed and built. This paper reports results of an experimental investigation of the unsteadiness induced by the stator on the relative flow leaving the centrifugal impeller.

The unsteady flow field at the impeller outlet, which is not axisymmetric due to the upstream potential effect of the vaned diffuser, has been investigated with a constant temperature hot wire anemometer for several relative circumferential positions of the probe and the diffuser in order to reconstruct in great detail instantaneous pictures of the rotor outflow periodically perturbed by the diffuser vanes in relative motion. To gain more insight into the upstream propagation mechanism of the stator induced unsteadiness, instantaneous static pressure at the front cover of the unshrouded impeller has also been measured using miniature fast response pressure transducers and has been processed to get the images of the periodically perturbed pressure field within the centrifugal impeller passages.

EXPERIMENTAL FACILITY AND OPERATING CONDITIONS

A simplified model of centrifugal turbomachine, dedicated to basic fluid dynamic studies, has been utilized for the present experimental investigation. The model is shown in Fig. 1.

The model consists of a 420 mm diameter unshrouded centrifugal impeller and a rotatable radial vaned diffuser which allows for continuous variation of the vaned diffuser circumferential location with respect to the measuring point. The impeller and the diffuser are shown in Fig. 2. The coordinates of the impeller blade and diffuser vane profiles are given in appendix.

The impeller, directly driven by an electric d. c. motor, has seven untwisted constant thickness backswept blades with rounded off leading and trailing edges. The blade camber angle with the radial direction varies continuously from 65 deg at the inlet ($D_1/D_2 = 0.57$) to 70 deg at the outlet, giving a geometrical diffusion ratio of 1.42. The diffuser is constituted by a disk with internal and external diameters 421 and 750 mm respectively, supported by a bearing plane. The disk can be rotated with respect to the support by means of circumferential slits and protruding pins. Constant thickness circular arc vanes can be used to construct several vaned diffusers with different vaneless radial gaps, stagger angles and number of vanes.

The diffuser used in the present investigation has 12 vanes and a 6 per cent vaneless radial gap. The front cover of the model, which constitutes the impeller and diffuser casing, is made of perspex to allow for flow visualization and easy probe positioning. The cover is supported by the bearing plane through eight cylindrical holders. The holders' height can be varied to change the blade tip clearance. In the present investigation the tip clearance is set at its minimum value of 0.4 mm, to reduce tip leakage effects.

The model operates in an open circuit, with air being fed to the impeller through a long straight pipe and discharged into the atmosphere directly from the radial diffuser. The inlet pipe is equipped with a honeycomb, a cloth filtering element and a throttling valve. The flow rate is measured by means of static pressure taps in the inlet pipe and a Pitot tube for the total pressure drop through the valve.

The experiment was conducted at the constant rotational speed of 2000

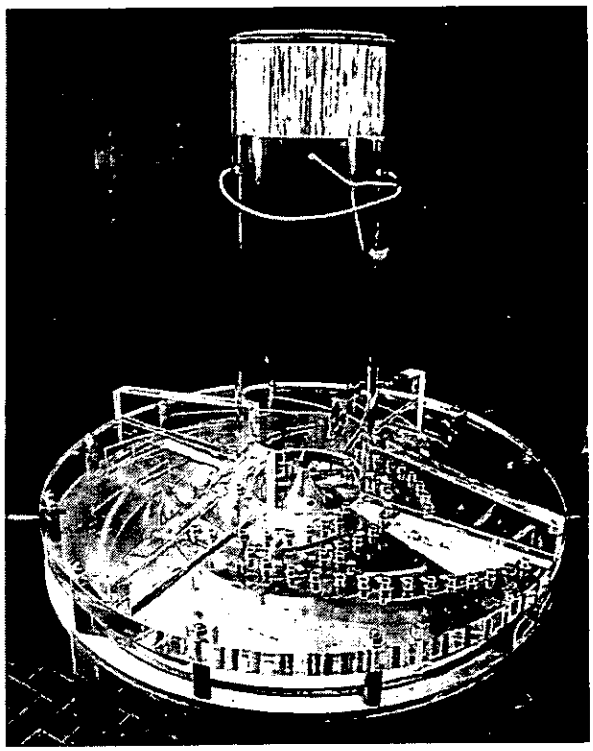

Fig. 1 Centrifugal turbomachine model

rpm, at the nominal operating condition (flow rate coefficient $\varphi = 0.048$, total pressure rise coefficient $\psi = 0.65$). At this operating condition the theoretical flow incidence on the impeller blades was 4 deg positive. The Reynolds number based on impeller tip speed and impeller blade chord was Re = 6.5 10^5. The main geometric data of the model and the operating conditions are summarized in Table 1.

INSTRUMENTATION AND MEASURING TECHNIQUES

A constant temperature hot wire anemometer with single sensor probes and flush mounted miniature fast response pressure transducers were used to measure the unsteady three-dimensional flow at the impeller outlet and the unsteady static pressure at the front cover facing the unshrouded impeller passages. To survey the impeller outflow, the hot wire probe was introduced from the front cover at a radial distance 4 mm from the blade trailing edge ($D_m/D_2 = 1.02$) and 8 mm from the vane leading edge.

The probe was traversed in axial direction to describe the impeller flow in spanwise direction with 17 measuring points. The minimum distance from the walls was 2 mm. During the impeller revolutions the stationary fast response hot wire probe senses an unsteady signal consisting of a periodic part and a random one. The former is due to the circumferential non uniformity of the relative flow, the latter is associated with flow turbulence, trailing edge vortex shedding, separations and all the other unsteady phenomena not correlated with the impeller frequency. This apparent turbulence can more properly be

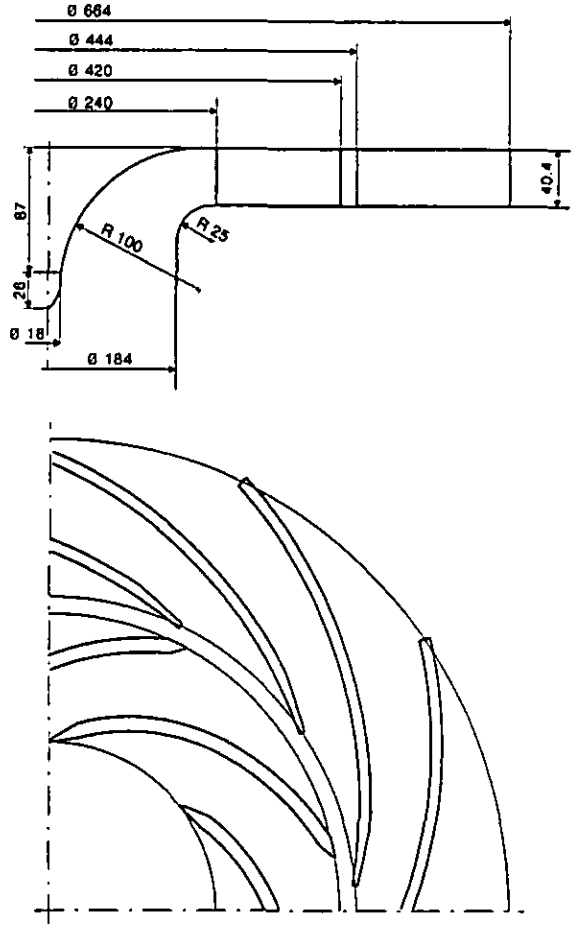

Fig. 2 Impeller and vaned diffuser geometry

Table 1 Geometric data and operating conditons

Impeller			
inlet blade diameter	D_1	=	240 mm
outlet diameter	D_2	=	420 mm
blade span	b	=	40 mm
number of blades	z_i	=	7
inlet blade angle (with radial direction)	β_1'	=	-65 deg
outlet blade angle	β_2'	=	-70 deg
Diffuser			
inlet vane diameter	D_3	=	444 mm
outlet vane diameter	D_4	=	664 mm
vane span	b	=	40 mm
number of vanes	z_d	=	12
inlet vane angle	α_3'	=	-74 deg
outlet vane angle	α_4'	=	-68 deg
Operating conditions			
rotational speed	n	=	2000 rpm
flow rate coefficient	φ	=	0.048
total pressure rise coefficient	ψ	=	0.65
Reynolds number	Re	=	$U_2 l/\nu$ = 6.5 10^5
Inlet air reference conditions			
temperature	T	=	298 K
air density	ρ	=	1.2 kg/m^3

defined as unresolved unsteadiness (Suder et al., 1987).

In order to separate the periodic signal from the unresolved unsteadiness, the phase locked sampling and ensemble average technique (Gostelow, 1977; Lakshminarayana, 1981) was applied to the hot wire instantaneous signals. The once per revolution reference signal was provided by an optical device which consists of a light source, a reflecting element glued on the shaft and a receiving photocell. The ensemble averages were obtained by averaging 700 records of 160 data, correspooding to 160 circumferential positions in the rotor reference. The instantaneous signals were digitized at a frequency rate of 18.667 kHz by means of a 12 bit A/D converter board and a trigger alarm module (Burr Brown PCI 20019M and 200020M) and the data were stored in a personal computer. The selected sampling frequency provides a detailed description of an impeller passage by means of 80 circumferential points.

Miniature normal and slanted single sensor probes (Dantec 55P11 and 55P12) with tungsten wires of 1.25 mm length and 5 μm diameter were used to measure instantaneous velocities. The frequency response of the system exceeds 100 kHz. The probes were accurately calibrated for velocity magnitude and direction. The instantaneous cooling velocities were obtained from the sampled signals by numerical inversion of the calibration curve.

For each measuring point a set of 12 ensemble averaged cooling velocities and 12 variances (9 for the slanted probe and 3 for the normal probe) were obtained by rotating the probe around the axis. The three ensemble averaged velocity components and the six apparent Reynolds stress components associated with the unresolved flow unsteadiness were determined using the above mentioned set of data and solving two overdetermined systems of algebraic equations. This experimental procedure is the same as the one used by Ubaldi et al. to measure the relative flow and turbulence characteristics downstream of a centrifugal

impeller (1993a) and an axial flow rotor (1993b). The details of the hot wire technique are given by Perdichizzi et al. (1990).

The instantaneous static pressure distributions at the front end of the unshrouded impeller were obtained at 10 radial measuring locations from the impeller inlet to the outlet, by combination of stationary and dynamic pressure measurements. The static pressure fluctuations were measured by means of a flush mounted semiconductor transducer (Entran Epil-203-013G) with a resonance frequency of 100 kHz. The time averaged static pressures were measured by means of static pressure taps and a Betz micromanometer to avoid thermal zero drift effects on the miniature semiconductor pressure transducer output. The instantaneous static pressure distributions were ensemble averaged using the same procedure as the one applied to the hot wire signals.

From verification tests performed in a calibration wind tunnel, the following experimental uncertainties have been estimated:

Mean velocity	±	1 per cent
Flow angles	±	1 deg
Apparent turbulence intensity	±	5 per cent
Static pressure	±	2 per cent of the reference inlet pressure
Probe position	±	0.1 mm

DATA REDUCTIDN

The ensemble average procedure enables the separation of the periodic unsteadiness at the blade passing frequency from the random unsteadiness, thus allowing to reconstruct the circumferential distribution of the impeller outflow velocity components in the relative frame, starting from the signal of a stationary probe. In case of vaneless diffuser or vaned diffuser with a large vaneless radial gap, the results are independent of the circumferential location of the probe. Reducing the radial distance between the probe and the vane leading edge lets the velocity distributions become sensitive to the probe circumferential location, as shown by Krain (1981) and by Inoue and Cumpsty (1984).

Evidence of the upstream potential flow effect generated by the vaned diffuser is given in Fig. 4. In the case of a vaned diffuser, a comprehensive description of the relative flow should account for information from several circumferential stationary points of view. In the present investigation, velocity and pressure measurements are taken at 30 circumferential locations distributed over one diffuser vane circumferential pitch, in such a way to achieve an accurate description of the unsteady flow also in space.

In the present investigation the probe is maintained at a fixed position with respect to the absolute frame of reference and the various relative probe-diffuser vane positions have been obtained by rotation of the diffuser. Thus the temporal coordinate of the instantaneous signal for each diffuser position corresponds to the same circumferential coordinate in the rotating frame of reference, regardless of the diffuser position.

Therefore the instantaneous signal (for instance the velocity c) is a function of time (t_j) or rotor circumferential coordinate, of the data record (n), of the stationary probe circumferential position with respect to the diffuser vane (θ_k) and of a further spatial coordinate (the axial coordinate (z) for the velocity measurements at the impeller outlet, the radial coordinate (r) for the pressure measurements at the impeller front end).

Omitting, for simplicity, the second spatial coordinate, the equations defining the ensemble average procedure are as follows:

instantaneous velocity

$$c_{njk}(t_j,\theta_k) = \bar{c}_{jk}(t_j,\theta_k) + c'_{njk}(t_j,\theta_k) \tag{1}$$

ensemble averaged velocity

$$\bar{c}_{jk}(t_j,\theta_k) = \frac{1}{N}\sum_{n=1}^{N} c_{njk}(t_j,\theta_k) \tag{2}$$

root mean square of the random unsteady fluctuations

$$\sqrt{\overline{c'^2_{jk}(t_j,\theta_k)}} = \sqrt{\frac{1}{N}\sum_{n=1}^{N}[c_{njk}(t_j,\theta_k) - \bar{c}_{jk}(t_j,\theta_k)]^2} \tag{3}$$

where $n = 1 \ldots N$ is the index of the sequence of records to be ensemble averaged ($N = 700$);
$j = 1 \ldots J$ is the index of the time coordinate t or the order of the sampled signal in the record ($J = 160$);
$k = 1 \ldots K$ is the index of the circumferential position θ of the probe ($K = 30$).

Inoue and Cumpsty (1984) for the case of a centrifugal compressor and Hathaway et al. (1987) for an axial compressor were able to divide the ensemble averaged velocity $\bar{c}_{jk}(t_j,\theta_k)$ into a steady state velocity and a rotor generated unsteadiness, by time averaging. This description has been proved to be effective in the study of the diffuser flow disturbed by the rotor wakes.

In the present study, concerning the upstream effect of the vaned diffuser on the rotor flow, the circumferential average over a diffuser vane pitch is performed instead of the time average. A representative picture of the impeller flow is provided in fact by the circumferential ensemble averaged velocity which is obtained by averaging the K distributions of the ensemble averaged velocity:

$$\bar{\bar{c}}_j(t_j) = \sum_{k=1}^{K}[\bar{c}_{jk}(t_j,\theta_k)\Delta\theta_k] \;/\; \sum_{k=1}^{K}\Delta\theta_k \tag{4}$$

The ensemble averaged velocity $\bar{c}_{jk}(t_j,\theta_k)$ can be split into two components: the circumferential ensemble averaged component $\bar{\bar{c}}_j(t_j)$ and the circumferential distributed fluctuating component $\bar{c}'_{jk}(t_j,\theta_k)$. The former is still a function of time or of the rotor circumferential coordinate and is no more dependent on the vane position. The latter is due to the upstream effect of the vaned diffuser on the steady, but not uniform in space, rotor relative flow.

$$\bar{c}_{jk}(t_j,\theta_k) = \bar{\bar{c}}_j(t_j) + \bar{c}'_{jk}(t_j,\theta_k) \tag{5}$$

The root mean square of the circumferential distributed fluctuating component $\bar{c}'_{jk}(t_j,\theta_k)$ represents the stator induced unsteadiness on the impeller flow:

$$\sqrt{\overline{\bar{c}'^2_j(t_j)}} = \sqrt{\sum_{k=1}^{K}[\bar{c}_{jk}(t_j,\theta_k) - \bar{\bar{c}}_j(t_j)]^2\Delta\theta_k \;/\; \sum_{k=1}^{K}\Delta\theta_k} \tag{6}$$

The concept of stator induced unsteadiness can be used to quantify the effects of the upstream propagation of the stator potential flow perturbation into the rotor flow. Furthermore the procedure of splitting the instantaneous velocity into a steady state velocity, a stator induced unsteadiness and an unresolved unsteadiness is suitable to be applied also to the Navier-Stokes equations in order to obtain an averaged form useful for simulating the steady state turbulent rotor flow periodically perturbed by the downstream vanes.

Figure 5 shows the circumferential ensemble averaged velocity and compares the stator induced unsteadiness with the unresolved unsteadiness (rms normalized by the impeller tip speed).

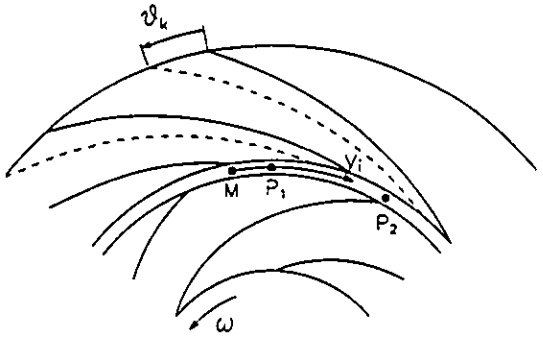

Fig. 3 Sketch of the radial rows of blades and reference coordinates

A more impressive description of the periodically unsteady rotor flow can be achieved by correlating in both time and space each measurement, in such a way to obtain an instantaneous relative flow field pattern, which can be displayed over several rotor passages, as shown by Binder et al. (1985), or represented over one or two rotor pitches for different time instants corresponding to different relative positions between impeller blades and diffuser vanes, as shown by Inoue and Cumpsty (1984).

In order to reconstruct the distribution of the ensemble averaged velocity $\bar{c}$ in function of the relative frame circumferential coordinate y_i at the time instant $\bar{t}$, it is necessary to reorder the information contained in the individual ensemble averaged signals obtained with the probe fixed in the point M for different circumferential positions θ_k of the diffuser.

Referring to Fig. 3, let P_m be the point in the m-th diffuser passage, whose circumferential coordinate in the relative frame is defined by

$$y_i(P_m) = \omega r \bar{t} + r\theta_k + (m-1)\frac{2\pi r}{z_d}$$

then the value of $\bar{c}$ in P_m at the time instant $\bar{t}$ can be obtained by interpolation of the function $\bar{c}_{jk}(i_j, \theta_k)$ at the temporal coordinate

$$t = \bar{t} + \frac{\theta_k}{\omega} + (m-1)\frac{2\pi}{z_d\omega}$$

Figure 7 shows a typical result of the described procedure. The distribution of the radial velocity versus the rotor circumferential coordinate is perturbed in proximity to the diffuser vanes; both the vanes and the perturbations, felt by a relative observer, move jointly in time.

RESULTS AND DISCUSSION

The results are given in terms of ensemble averaged and circumferential ensemble averaged velocity components and pressures, as well as of unresolved and stator generated unsteadiness distributions in space and time.

All the kinematic quantities are normalized with the rotor tip speed U_2. The circumferential rotor relative coordinate y_i and the axial coordinate z are made nondimensional by means of the rotor circumferential pitch $G_i=2\pi r/z_i$ and the blade span at the rotor outlet b, respectively. The circumferential position of the probe with respect to the vane leading edge θ is normalized by the angular pitch of the diffuser $2\pi/z_d$. The time t is divided by the rotor blade passing period $T_i = 2\pi/\omega z_i$.

Ensemble averaged velocity and stator generated unsteadiness

Figure 4 shows the ensemble averaged relative velocity distributions versus time. These results were obtained at midspan, for $D_m/D_2 = 1.02$, with the stationary probe located in two different circumferential positions with respect to the rotatable diffuser. The probe senses in time sequence first the pressure side, then the wake and finally the impeller passage from the suction to the pressure side. When the probe is set near midpitch ($\theta\, z_d/2\pi = 0.4$) the diagram shows a typical circumferential distribution of an unseparated outflow with clear evidence of blade wake velocity defects, velocity peaks at the pressure side blade trailing edges and negative velocity gradient from suction to pressure side through the passage. The vane position has an important influence on the measurement results. When the probe is in proximity of the vane leading edge ($\theta z_d/2\pi = 0$), the pressure side peak is enhanced, whereas the velocity is depressed on the suction side and the impeller passage velocity gradient has completely altered.

The ensemble averaged distributions corresponding to each of the 30 circumferential positions of the probe were circumferentially averaged and the result is plotted on the top of Fig. 5 in function of the normalized rotor circumferential coordinate. The resulting distribution looks very smooth and shows a good periodicity. It conserves the pressure side peaks and wake deficits already observed. The wake extends on the suction side more than on the pressure side and from the suction side the relative velocity continuously increases till mid-passage, where a large smooth maximum is formed.

The same figure also reports the comparison of the stator generated unsteadiness and the circumferentially averaged unresolved unsteadiness. Both quantities are relevant and comparable. Peaks of 7 and 8 per cent of the peripheral rotor speed are displayed by the stator induced and the unresolved unsteadiness respectively. Since the mean relative velocity is about 60 per cent of the peripheral speed, these values correspond to apparent turbulence intensities larger than 10 per cent. The unresolved unsteadiness presents a peak at the wake centre position. From this point the unsteadiness decreases continuously through the suction side region to about a value of 2.5 per cent. A minimum is located in correspondence with the pressure side velocity peak and from this position the unresolved unsteadiness has a steep increase which gives rise to the wake peak.

The stator generated unsteadiness shows a characteristic twin peak configuration in the wake region with a minimum at the wake centre, in opposition to the unresolved unsteadiness maximum. The stator generated unsteadiness decreases continuously through the impeller passage, from the suction to the pressure side regions, with values that vary from 5 to less than 2 per cent. This result is rather interesting as it means that the centre of the wake and the pressure side of the passages

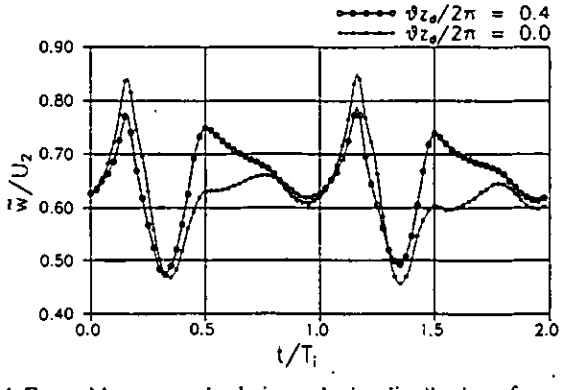

Fig. 4 Ensemble averaged relative velocity distributions for two different circumferential locations of the probe, at the impeller outlet, midspan position

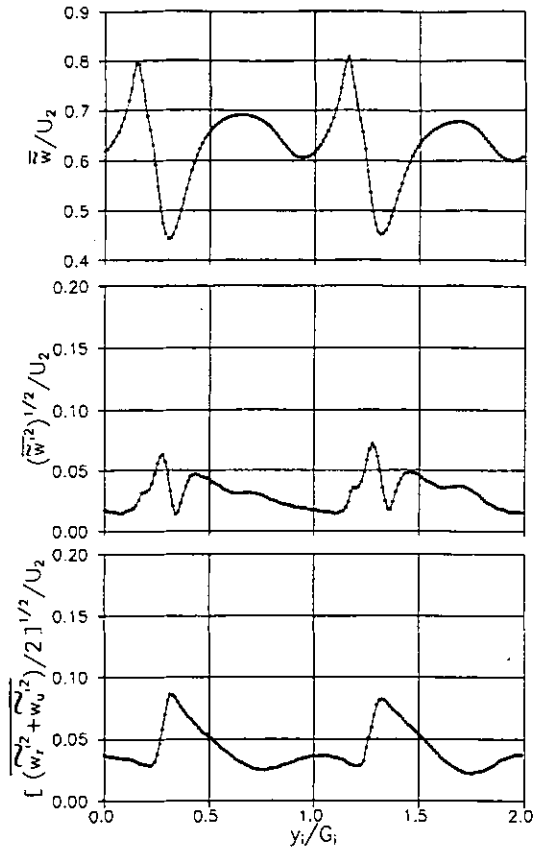

Fig. 5 Circumferential ensemble averaged relative velocity, stator generated unsteadiness and unresolved unsteadiness at the impeller outlet, midspan position

are nearly unaffected by stator induced unsteadiness, implying that they represent a limit to the propagation of the stator induced unsteadiness to adjacent rotor passages.

In order to have an overall representation of the mean unsteady flow field, the results obtained from the 17 spanwise measuring locations are used to construct area plots depicted over the cylindrical section of the model at the impeller outlet (Fig. 6). The physical scale of the frame is modified such that the vertical scale is 3 times the horizontal one. The impeller blades move from right to left.

The grey filled contours of the circumferentially ensemble averaged relative velocity, the contours of the stator induced unsteadiness, and the circumferentially averaged relative secondary velocity vectors are shown in Fig. 6. Secondary velocity components are those in the plane perpendicular to the primary direction defined by the flow in the centre of the passage (β = -76 deg, γ = 0 deg).

In the plot of the mean relative velocity, the two dark grey filled area, representing the traces of the blade wakes, extend in spanwise direction from hub to tip separating the individual impeller passages. Narrow light grey bands parallel to the wake traces show a relative velocity increase around the pressure side trailing edge region. The mean relative velocity increases continuously from the wake suction side toward mid passage.

The contours give also evidence of a core of rather low momentum fluid, approximately located near midspan, halfway between the mid-passage and the pressure side of the passage. This throughflow momentum wake, characteristic of unshrouded centrifugal impellers (e.g. Krain, 1987; Hathaway et al., 1993), is mainly due to the tip leakage action which produces losses and convects them toward the pressure side, as also shown by results of calculations on a low-speed centrifugal compressor (Moore and Moore, 1993).

A second region of low momentum fluid has been formed on the suction side/hub corner. In the present model, with the blades set in the wholly radial part of the impeller, the Rossby number $Ro = w/\omega R_n$, as defined by Johnson (1978), tends to zero. The centrifugal force defect acting on the blade boundary layers becomes negligible when compared with the Coriolis force effect on the hub endwall. This low momentum fluid is convected into the suction side/hub corner by the passage vortex and this stable location for the wake is maintained.

Evidence of the passage and tip leakage vortices is given by the residual secondary velocities of the mean relative flow, which can be observed at the hub and casing endwalls respectively, in the vector plot of Fig. 6. The same vector plot also shows that, close to the wakes, relevant secondary slip velocities move against the rotor speed and feed fluid from the pressure side of the passage into the blade wake.

The unsteadiness generated by the stator on the impeller outflow is shown at the middle of Fig. 6. The narrow vertical dark grey bands extending from the hub to the casing in the centre of the wakes constitute clean circumferential discontinuities in the stator generated unsteadiness distribution. This unsteadiness is large on both the pressure and suction sides of the wake, but low in the wake centre. Within the impeller

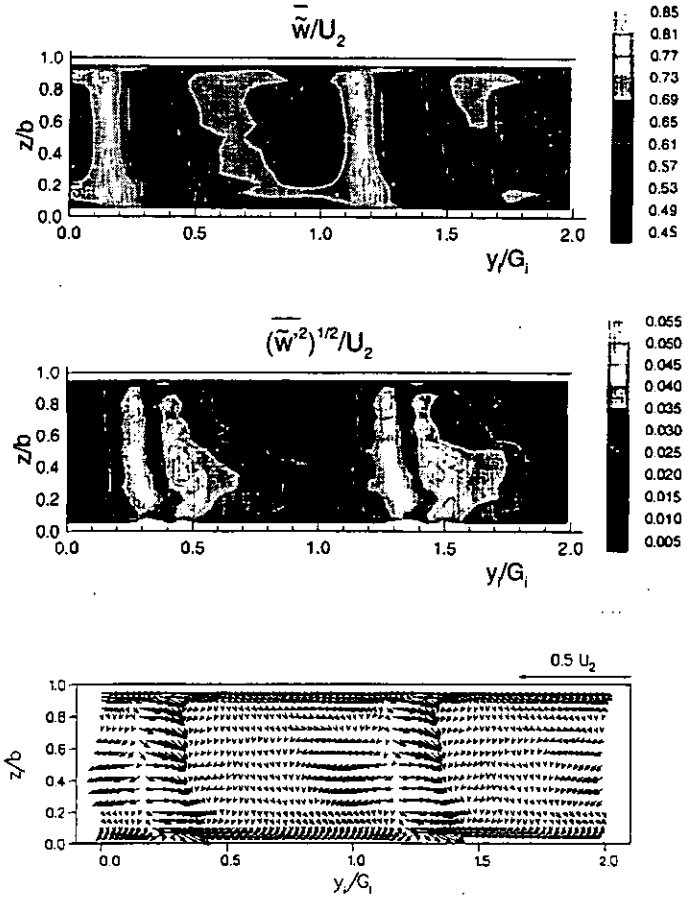

Fig. 6 Circumferential ensemble averaged relative velocity, stator generated unsteadiness and circumferential averaged relative secondary velocities at the impeller outlet

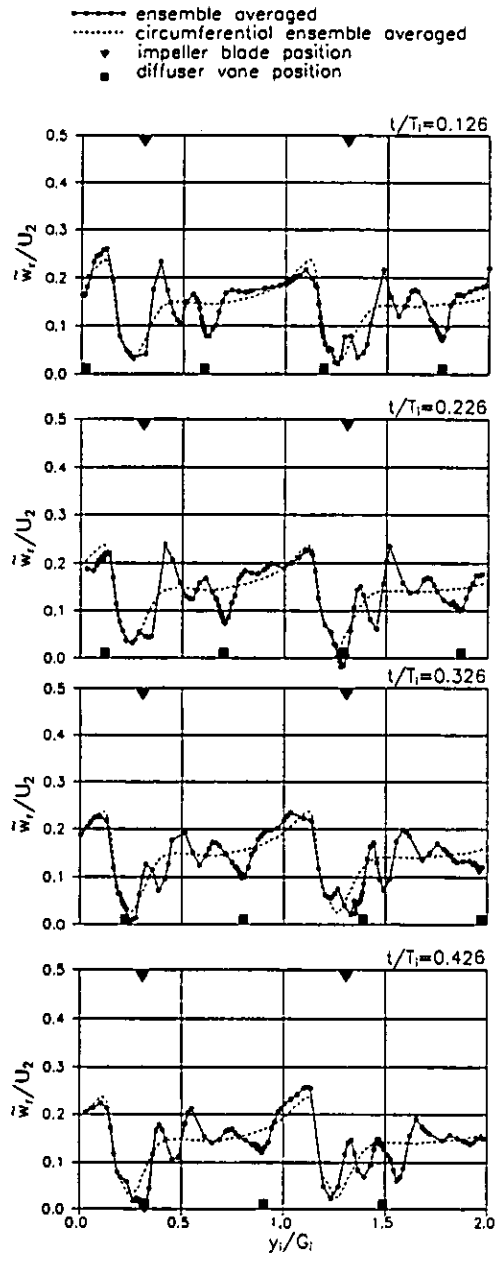

Fig. 7 Instantaneous distributions of the ensemble averaged radial velocity at the impeller outlet, midspan position

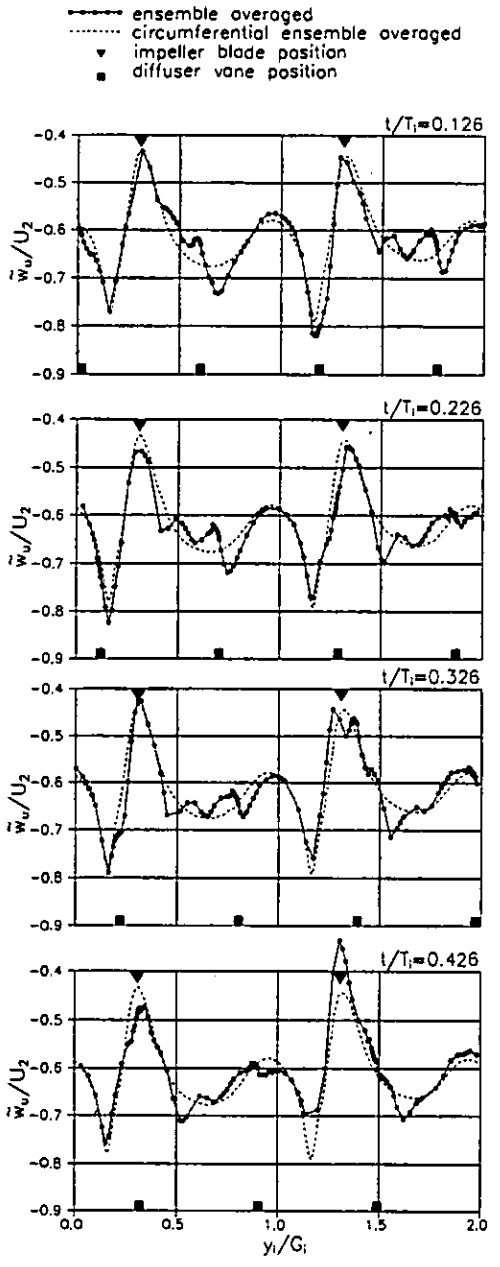

Fig. 8 Instantaneous distributions of the ensemble averaged tangential relative velocity at the impeller outlet, midspan position

passage, the unsteadiness decreases from the suction to the pressure side and it is more intense between midspan and the hub endwall.

Instantaneous distributions of the ensemble averaged velocity components

Figure 7 shows the instantanenus circumferential distributions of the ensemble averaged radial velocity at midspan, observed in the relative frame, for four different relative positions of the impeller blades and the diffuser vanes. For clarity the circumferential positions of blades and vanes are marked at the top and bottom of each frame respectively. In the relative frame of reference, the impeller blade traces and the associated wakes have a fixed position in time, while the diffuser vanes are seen to move at the impeller peripheral speed, but in opposite direction, from left to right. To highlight the stator induced unsteady disturbances, the circumferential ensemble averaged radial velocity is plotted with dashed line over each instantaneous distribution.

The radial velocity distributions display well defined minima on the pressure side of the wakes. The circumferential misalignment between the blade traces located in the centre of the wakes and the radial velocity minima depends on the distribution of the relative flow angle which has its minimum just on the pressure side of the wake. The diffuser generated upstream potential flow effect is such that the radial velocity in proximity to each vane leading edge presents a local minimum. These minima rotate jointly with the diffuser vanes. The stagnation effect induces local reversals of the flow, whenever the impeller blade trailing edge and the diffuser vane leading edge are circumferentially aligned.

An interesting feature observable from the variations of the radial velocity distribution with time is the presence of a series of peaks and

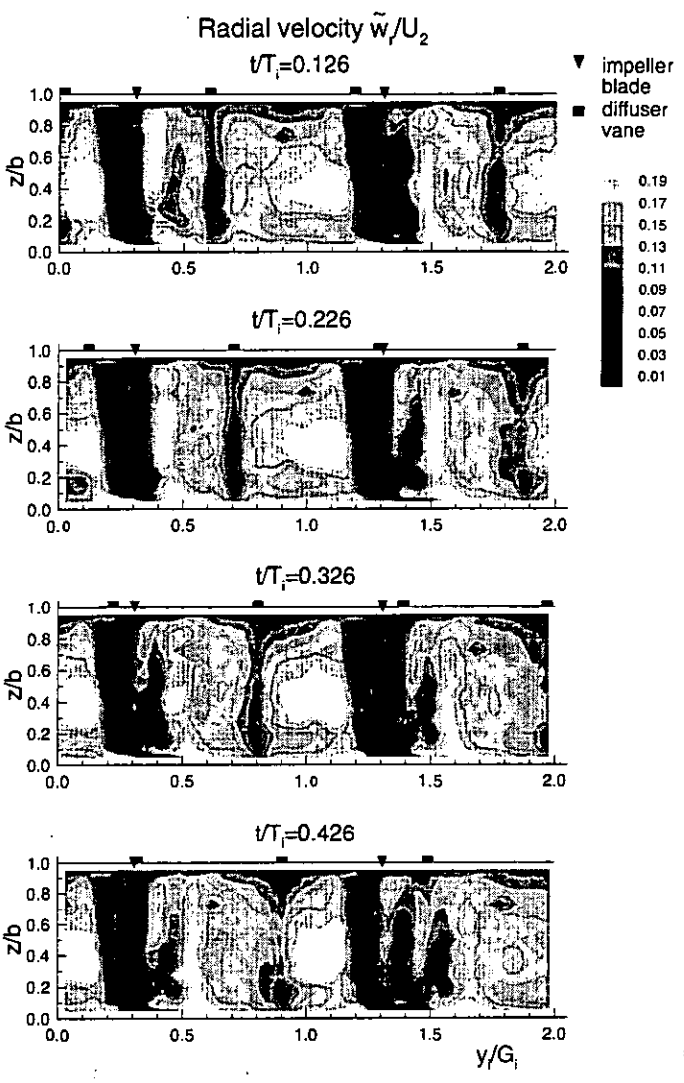

Fig. 9 Instantaneous pictures of the ensemble averaged radial velocity at the impeller outlet

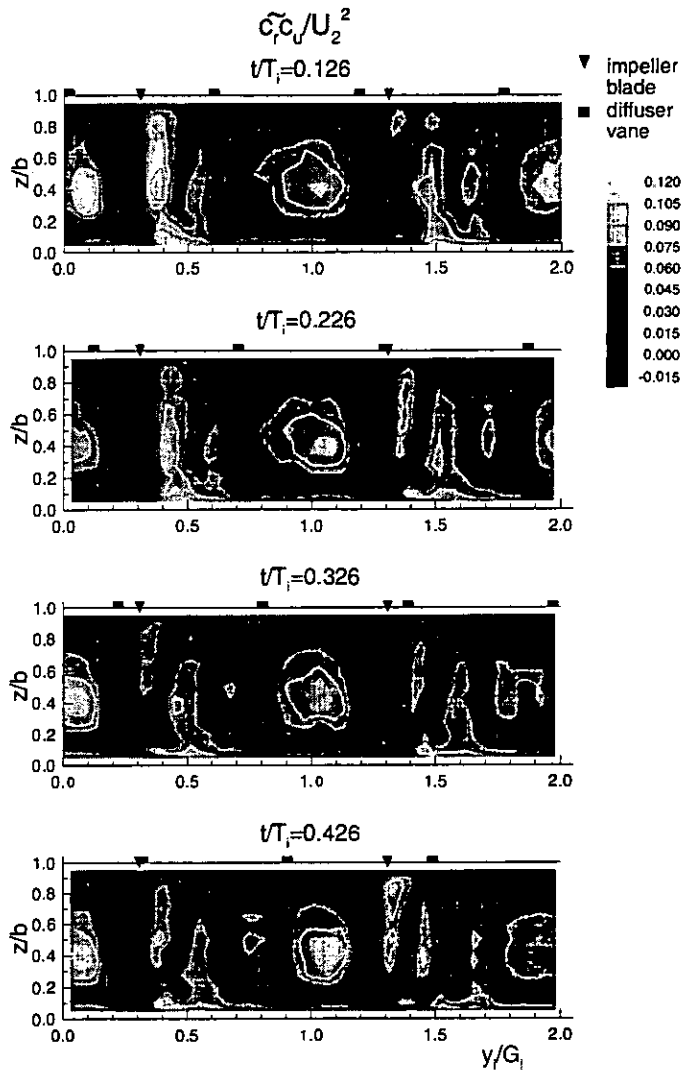

Fig. 10 Instantaneous pictures of the ensemble averaged non dimensional moment of momentum of flow rate at the impeller outlet

valleys which originate on the suction side of the impeller passage and follow the leading minimum corresponding to the diffuser vane.

These disturbances propagate in circumferential direction with a velocity of -0.6 U_2, approximately equal to w_u, and reduce their amplitude with time. An explanation of this phenomenon has not yet been obtained, but the above mentioned features suggest that they may be associated with the transit, in the measuring station, of flow which has been previously perturbed within the impeller by the passing diffuser vanes.

All the observed disturbances, correlated with the diffuser vane transit, reduce their amplitude from the suction to the pressure side of the impeller passage, in accordance with the previously shown stator induced unsteadiness distribution.

The instantaneous distributions of the ensemble averaged relative velocity tangential component, given in Fig. 8, show variations through the blade wakes of about 35 per cent of the peripheral speed U_2. The minimum, which is about -0.8 U_2, is located on the pressure side, outside of the wake, where a peak of the relative velocity has been already observed. The maximum (about -.45 U_2) is aligned with the centre of the wake.

The perturbations induced by the diffuser vanes are evidenced by tangential velocity variations on the vane sides. In fact the absolute streamlines tend to deflect around the vane leading edge, with an increase of the tangential velocity component on the suction side and a decrease on the pressure side of the diffuser vane leading edge. This effect was also observed by Inoue and Cumpsty (1984).

Instantaneous pictures of the ensemble averaged velocity field at the impeller outlet, as seen by a relative observer, have been reconstructed from the data taken at the 17 axial measuring stations. The radial velocity distributions are shown in Fig. 9, as grey filled contour plots. The impeller blades are fixed with time and the diffuser vanes appear to move past with circumferential speed -U_2. The radial velocity field is dominated by the presence of regions of very low velocity located on the pressure side of the blade traces and fixed with them in time. Depending on the relative positions of the vanes, the radial velocity on the suction side of the blade wakes changes with time from high to low values. For instance, when the diffuser vane is situated on the suction side of the impeller wake (t/T_i = 0.326, second blade from left), the

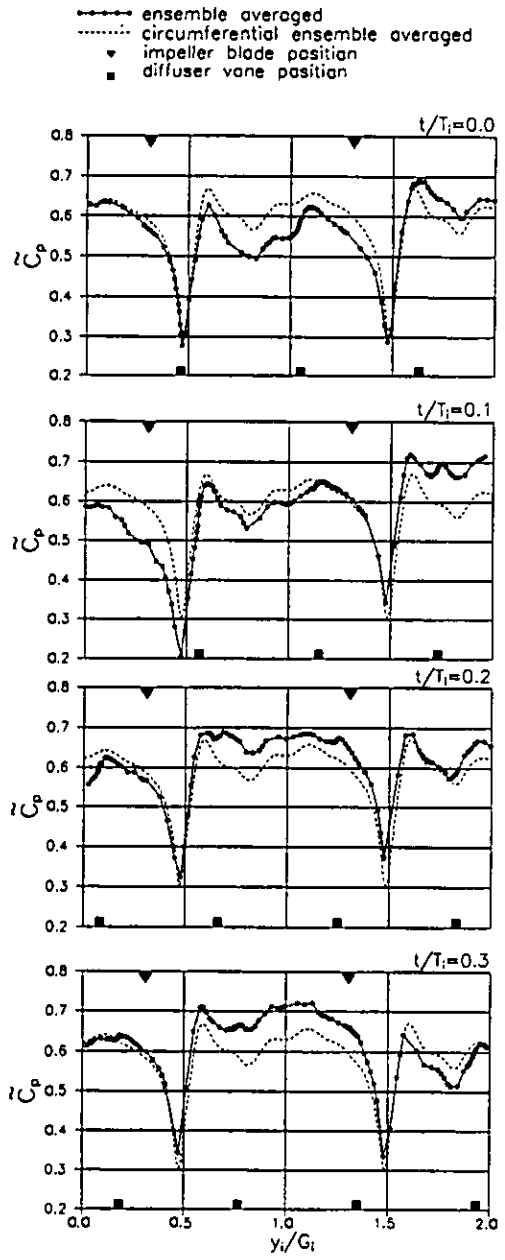

Fig. 11 Instantaneous distributions of the ensemble averaged static pressure coefficient at the impeller outlet

defect in radial velocity becomes wider and the wake appears enlarged.

Looking at the central impeller passage, a well defined deep velocity defect corresponding to the diffuser vane is evident. This interaction effect appears even more pronounced in the regions closer to the endwalls. As already observed, the main perturbation is followed by a series of smoother valleys and peaks moving from pressure to suction side with reduced speed and further perturbing the velocity field.

Since the potential effect of the vaned diffuser perturbs the instantaneous kinematic field at the impeller outlet, a remarkable effect should also be expected on the moment of momentum of the fluid leaving the impeller. Figure 10 shows instantaneous pictures of the nondimensional quantity $\widetilde{c_t}\widetilde{c_u}/U_2^2$, which is proportional to the moment of momentum of the mass flow rate leaving the impeller. This term represents an important contribution to the local rotor work exchange. In case of steady flow in the rotating frame and shrouded impeller its integral over the exit area of the impeller is proportional to the impeller power input. When, as in the present case, the flow is unsteady in the relative frame and the impeller is unshrouded, the power loss due to viscous friction on the casing and the time rate of change of moment of momentum in the control volume should also be taken into account when calculating the impeller power (Lyman, 1993).

The plots of Fig. 10 show relevant circumferential and instantaneous variations of $\widetilde{c_t}\widetilde{c_u}/U_2^2$. The energy exchange is very low on the pressure side of the impeller blades where both radial and tangential absolute velocities are low. On the contrary, the suction side of the wake and the core of low relative velocity, located near midspan, at the passage pressure side, are regions of large energy exchange.

The stator generated unsteady effect continuously modifies the instantaneous flow pattern. The energy exchange is reduced at the pressure side of the diffuser vane due to the reduction of both radial and absolute tangential velocities in that region. As expected, this disturbance moves jointly with the vane. When the vane approaches the impeller pressure side from mid-passage, the core of intense energy exchange, compressed between the vane and the pressure side of the wake, progressively reduces its area while its intensity tends to increase.

A further remarkable unsteady effect can be observed on the blade suction side region which, at $t/T_i = 0.126$, shows the largest values of

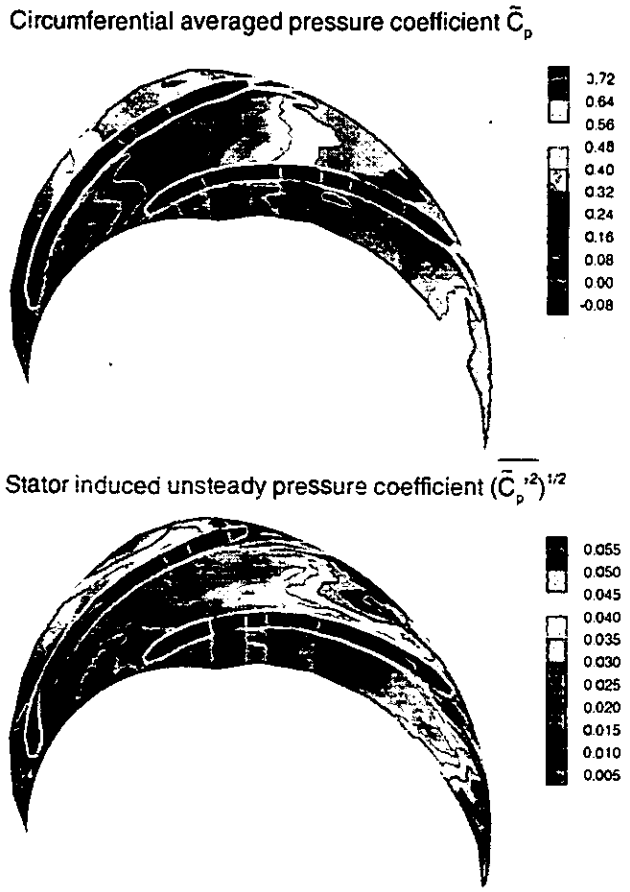

Fig. 12 Circumferential ensemble averaged static pressure coefficient and stator generated unsteady pressure coefficient at the impeller front end

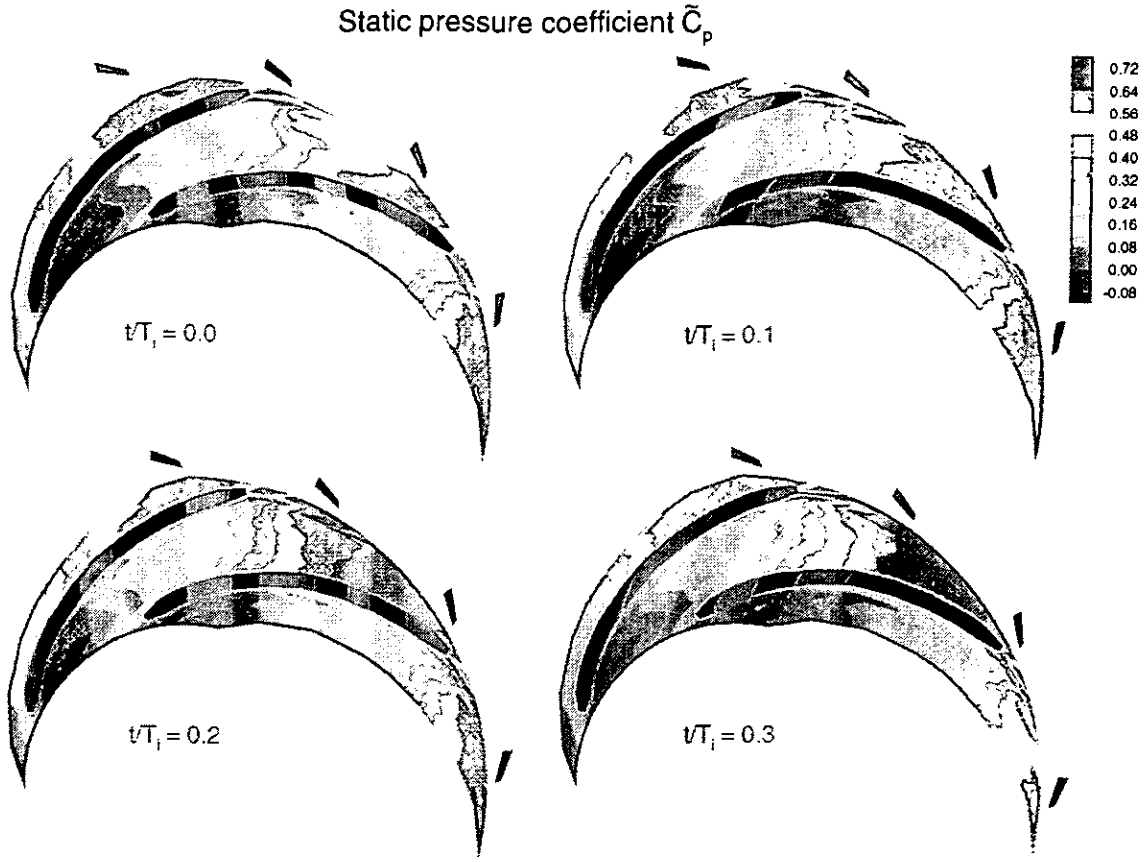

Fig. 13 Instantaneous pictures of the ensemble averaged static pressure coefficient at the front end of the impeller

the local energy exchange, but at $t/T_i = 0.426$ presents local reductions of more than 30 per cent.

Pressure distributions

Unsteady pressure measurements at the unshrouded impeller front end were made for ten pressure taps from the impeller inlet to the outlet. Figure 11 shows the instantaneous distributions of the ensemble averaged pressure coefficient $\tilde{C}_p$, measured at the same radial station (D_m/D_2 = 1.02) as the velocity. The instants chosen to describe the time evolution of the pressure are different from those chosen for the velocity, but the reference initial time ($t/T_i = 0$) is the same for all quantities. To point out the unsteady effects generated by the diffuser, the circumferential ensemble averaged pressure distribution is added to each diagram.

The most striking feature of these distributions is the fact that the upstream disturbance induced by the diffuser vanes is not localized and does not rotate with the diffuser vane, as in the case of the velocity. On the contrary, it influences the whole pressure field limited by the two lateral pressure minima. In each impeller passage, the pressure fluctuates in time with a period of $T = 0.583\ T_i$, equal to the vane passing period, and an amplitude of about 8 per cent of the dynamic pressure associated with the impeller speed U_2. This amplitude corresponds to pressure fluctuations as large as 25 per cent of the impeller pressure rise with high and low pressure levels alternating in the same passage and from a passage to the adjacent one.

For each radial measuring location, the circumferential ensemble averaged pressure coefficient $\overline{\tilde{C}_p}$ and stator generated unsteady pressure coefficient $(\overline{\tilde{C}_p'^2})^{1/2}$ were calculated. The spatial distributions of the two pressure coefficients are given in Fig. 12, as colour filled contours depicted over the impeller passages. The impeller rotates counter clockwise.

Since impeller endwalls are straight, blade span is small compared with blade chord, and tip clearance is small too, the pressure measurements at the impeller front end are representative of the pressure distribution in the impeller passages (Gostelow, 1977).

As expected, the pressure increases along the impeller channel, showing characteristic potential flow features such as a remarkable blade aerodynamic loading, a stagnation effect on the pressure side of the leading edge region, a local minimum in the suction side region and, above all, an important pressure rise in the semi-vaneless region at the impeller outlet.

The stator induced pressure unsteadiness propagates into the impeller undergoing progressive reduction nearly linear with the radial distance. At the impeller outlet the unsteady pressure coefficient takes values greater than 0.05, corresponding to an effective pressure unsteadiness of about 8 per cent of the impeller pressure rise. At the impeller inlet the unsteady pressure coefficient is reduced to less than 0.01.

The instantaneous pictures of the ensemble averaged static pressure coefficient $\tilde{C}_p$ of Fig. 13 show remarkable variations with time in the semi-vaneless region at the impeller outlet. Referring tn the central impeller passage, the pressure level is low at the instant $t/T_i = 0$, when the blade is approximately circumferentially centered in the diffuser passage. After a semi period of the diffuser vane passage, approximately corresponding to the time instant $t/T_i = 0.3$, the pressure level in the

semi-vaneless region of the impeller and at the pressure side of the blade becomes high. In that instant the blade trailing edge and the vane leading edge are approximately aligned in the radial direction and their distance is minimum.

CONCLUSIONS

To study the upstream potential flow effect induced by the vaned diffuser on the impeller flow, detailed velocity and pressure measurements were performed with stationary fast response probes in a simplified model of centrifugal turbomachine.

The flow has been investigated for several relative circumferential positions of the probe with respect to the vaned diffuser. Data have been reduced and analysed by means of ensemble average and circumferential ensemble average techniques in order to separate the periodic contribution due to steady non uniform flow in the impeller from the unresolved and the stator generated unsteadiness. This latter unsteady contribution has been calculated as the rms of the unsteady periodic fluctuations due to the diffuser vanes which are in relative motion with respect to the impeller passages.

At the impeller outlet the unresolved and the stator generated unsteadiness are comparable and present peaks of about 10 per cent of the relative velocity. The stator generated unsteady pressure coefficient at the impeller outlet is about 8 per cent of the impeller pressure rise and propagates upstream into the impeller with a reduction proportional to the radial distance from the diffuser vanes.

By correlating in space and time the large amount of data taken, instantaneous pictures of the rotor outflow and of the impeller pressure distribution have been obtained. These pictures show the details of the flow periodically perturbed by the diffuser vanes.

Relevant local defects of radial velocity and streamline deflections are induced on the flow at the impeller outlet by the vaned diffuser. The diffuser vanes and the local perturbations move jointly from the suction side of the passage followed by further flow disturbances that propagate circumferentially in time with the tangential relative velocity.

The periodic interaction of the stator generated flow perturbations with the local spatial non-uniformities of the impeller relative flow give rise to significant flow phenomena, such as periodic local reversed flow and instantaneous peaks of local work exchange.

The upstream diffuser effect on the static pressure results in a change of the pressure level in the whole impeller passage with time, rather than in a localized perturbation, as is the case for the velocity. Periodic pressure fluctuations as large as 25 per cent of the impeller pressure rise affect the impeller passage and propagate to the adjacent passages.

The investigation has been limited to just one geometry and one flow condition and therefore quantitative information can not be generalized. Nevertheless these detailed results provide a better understanding of the potential flow interaction phenomena and give an estimation of the importance of the different effects induced by the vaned diffuser on the impeller flow.

ACKNOWLEDGMENTS

This work has been carried out with the support of the Italian National Council of Research and the Ministry of University and Scientific Research.

REFERENCES

Arndt, N., Acosta, A. J., Brennen, C. E., and Caughey, T. K., 1990, "Experimental Investigation of Rotor-Stator Interaction in a Centrifugal Pump With Several Vaned Diffusers", ASME *Journal of Turbomachinery*, Vol. 112, pp. 98-108.

Binder, A., Forster, W., Kruse, H., and Rogge, H., 1985, " An Experimental Investigation Into the Effect of Wakes on the Unsteady Turbine Rotor Flow", ASME *Journal of Engineering for Gas Turbines and Power*, Vol. 107, pp. 458-466.

Binder, A., Schroeder, Th., and Hourmouziadis, J., 1989, "Turbulence Measurements in a Multistage Low-Pressure Turbine", ASME *Journal of Turbomachinery*, Vol. 111, pp. 153-161.

Dring, R. P., Joslyn, H. D., Hardin, L. W., and Wagner, J. H., 1982, "Turbine Rotor-Stator Interaction", ASME *Journal of Engineering for Power*, Vol. 104, pp. 729-742.

Dunker, R. J., 1983, " Flow Measurements in the Stator Row of a Single-Stage Transonic Axial-Flow Compressor with Controlled Diffusion Stator Blades", *Proceedings of the 61th AGARD Specialists' Meeting of the Propulsion & Energetics Panel on Viscous Effects in Turbomachines*, Copenhagen, Denmark, Paper 23.

Gostelow, J. P., 1977, "A New Approach to the Experimental Study of Turbomachinery Flow Phenomena", ASME *Journal of Engineering for Power*, Vol. 99, pp. 97-105.

Hathaway, M.D., Okiishi, T. H., Suder, K. L., Strazisar, A. J., and Adamczyk, J. J., 1987, "Measurements of the Unsteady Flow Field Within the Stator Row of a Transonic Axial-Flow Fan II - Results and Discussion", ASME Paper No. 87-GT-227.

Hathaway, M. D., Chriss, R. M., Wood, J. R., and Strazisar, A. J., 1993, "Experimental and Computational Investigation of the NASA Low-Speed Centrifugal Compressor Flow Field", ASME *Journal of Turbomachinery*, Vol. 115, pp. 527-542.

Hodson, H. P., 1985, "Measurements of Wake-Generated Unsteadiness in the Rotor Passages of Axial Flow Turbines", ASME *Journal of Engineering for Gas Turbines and Power*, Vol. 107, pp. 467-476.

Krain, H., 1981, "A Study on Centrifugal Impeller and Diffuser Flow", ASME *Journal of Engineering for Power*, Vol. 103, pp. 688-697.

Krain, H., 1987, "Swirling Impeller Flow", ASME Paper No. 87-GT-19.

Inoue, M., and Cumpsty, N. A., 1984, "Experimental Study of Centrifugal Impeller Discharge Flow in Vaneless and Vaned Diffusers", ASME *Journal of Engineering for Gas Turbines and Power*, Vol. 106, pp. 455-467.

Johnson, M. W., 1978, "Secondary Flows in Rotating Bends", ASME *Journal of Engineering for Power*, Vol. 100, pp. 553-560.

Joslyn, H. D., Dring, R. P., and Sharma, O. P., 1983, "Unsteady Three-Dimensional Turbine Aerodynamics", ASME *Journal of Engineering for Power*, Vol. 105, pp. 322-331.

La Graff, J. E., Ashworth, D. A., and Schultz, D. L., 1989, "Measurement and Modeling of the Gas Turbine Blade Transition Process as Disturbed by Wakes", ASME *Journal of Turbomachinery*, Vol. 111, pp. 315-322.

Lakshminarayana, B., 1981, "Techniques for Aerodynamic and Turbulence Measurements in Turbomachinery Rotors", ASME *Journal of Engineering for Power*, Vol. 103, pp. 374-392.

Liu, X., and Rodi, W., 1992, "Measurement of Unsteady Flow and Heat Transfer in a Linear Turbine Cascade", ASME Paper No. 92-GT-323.

Lyman, F. A., 1993, "On the Conservation of Rothalpy in Turbomachines", ASME *Journal of Turbomachinery*, Vol. 115, pp. 520-526.

Moore, J., and Moore J. G., 1993, discussion to the paper "Experimental and Computational Investigation of the NASA Low-Speed Centrifugal Compressor Flow Field", by Hathaway, M. D., Chriss, R. M., Wood, J. R., and Strazisar, A. J., ASME *Journal of Turbomachinery*, Vol. 115, pp. 541-542.

Perdichizzi, A., Ubaldi, M., and Zunino, P., 1990, "A Hot Wire Measuring Technique for Mean Velocity and Reynolds Stress Components in Compressible Flow", *Proceedings of the 10th Symposium on Measuring Techniques for Transonic and Supersonic Flows in Cascades and Turbomachines*, VKI, Brussels, Belgium, Paper 8.

Pfeil, H., Herbst, R., and Schroeder, T., 1983, Investigation of the Laminar-Turbulent Transition of Boundary Layers Disturbed by Wakes", ASME *Journal of Engineering for Power*, Vol. 105, pp. 130-137.

Poensgen, C., and Gallus, H. E., 1990a, "Three-Dimensional Wake Decay Inside of a Compressor Cascade and Its Influence on the Downstream Unsteady Flow Field. Part I: Wake Decay Characteristics in the Flow Passage", ASME Paper No. 90-GT-21.

Poensgen, C., and Gallus, H. E., 1990b, "Three-Dimensional Wake Decay Inside of a Compressor Cascade and Its Influence on the Downstream Unsteady Flow Field. Part II: Unsteady Flow Field Downstream of the Stator", ASME Paper No. 90-GT-22.

Schulz, H. D., Gallus, H. E., and Lakshminarayana, B., 1990, "Three-Dimensional Separated Flow Field in the Endwall Region of an Annular Compressor Cascade in the Presence of Rotor-Stator Interaction. Part 2 - Unsteady Flow and Pressure Field", ASME *Journal of Turbomachinery*, Vol. 112, pp. 679-690.

Suder, K. L., Hathaway, M. D., Okiishi, T. H., Strazisar, A. J., and Adamczyk, J. J., 1987, " Measurements of the Unsteady Flow Field Within the Stator Row of a Transonic Axial-Flow Fan I - Measurement and Analysis Technique", ASME Paper No. 87-GT-226.

Ubaldi, M., Zunino, P., and Cattanei, A., 1993a, "Relative Flow and Turbulence Measurements Downstream of a Backward Centrifugal Impeller", ASME *Journal of Turbomachinery*, Vol. 115, pp. 543-551.

Ubaldi, M., Zunino, P., and Cattanei, A., 1993b, "Relative Flow and Turbulence Measurements Downstream of an Axial Flow Rotor", *Engineering Turbulence Modelling and Experiments* 2, Rodi W. and Martelli F., ed., Elsevier Science Pub., pp. 795-804.

Zeschky, J., and Gallus, H. E., 1991, "Effects of Stator Wakes and Spanwise Nonuniform Inlet Conditions on the Rotor Flow of an Axial Turbine Stage", ASME Paper No. 91-GT-93.

Zierke, W. C., and Okiishi, T. H., 1982, "Measurement and Analysis of Total-Pressure Unsteadiness Data From an Axial-Flow Compressor Stage, ASME *Journal of Engineering for Power*, Vol. 104, pp. 479-488.

APPENDIX

Diffuser vane profile geometry

The diffuser vanes are thin constant thickness circular arc aerofoils. The geometry is defined by the following parameters:

- Radius of curvature of the camber line R_c = 332 mm.
- Angle between the camber line chord and the radial direction at the inlet λ_3 = 101.65 deg.
- Inlet and outlet radii of the camber line R_3 = 223.94 mm, R_4 = 332 mm.
- Constant thickness of the profile 8 mm.
  Reduced thickness at the leading edge 4 mm, obtained by a linear cut of the airfoil on the pressure side from 13 per cent of the camber line to the leading edge.

Impeller blade profile coordinates

Suction side		Pressure side	
R (mm)	θ (deg)	R (mm)	θ (deg)
120.00	0.00	120.00	0.00
120.48	1.61	122.76	1.16
121.06	3.21	124.91	2.79
121.74	4.79	126.76	4.10
122.50	6.36	128.71	5.40
123.36	7.91	130.77	6.69
124.31	9.43	132.95	7.96
128.31	13.62	137.43	11.86
132.58	17.67	141.73	15.98
136.86	21.65	146.03	20.04
141.13	25.60	150.33	24.05
145.40	29.50	154.63	28.03
149.67	33.37	158.92	31.96
153.94	37.21	163.22	35.86
158.22	41.01	167.52	39.72
162.49	44.79	171.81	43.54
166.77	48.52	176.11	47.33
171.05	52.22	180.40	51.06
175.33	55.87	184.69	54.75
179.61	59.47	188.98	58.39
183.89	63.02	193.27	61.97
188.17	66.52	197.56	65.49
192.45	69.95	201.85	68.95
196.74	73.31	206.13	72.34
201.02	76.61	210.42	75.66
203.83	77.59	210.34	77.00
206.67	78.52	210.36	78.23
209.53	79.42	210.47	79.33